
THE COOPERATIVE NETWORK ARCHITECTURE: LEARNING STRUCTURED NETWORKS AS REPRESENTATION OF SENSORY PATTERNS

Pascal J. Sager

Zurich University of Applied Sciences
University of Zurich
sage@zhaw.ch

Jan M. Deriu

Zurich University of Applied Sciences
deri@zhaw.ch

Benjamin F. Grewe

University of Zurich, ETH Zurich
bgrewe@ethz.ch

Thilo Stadelmann

Zurich University of Applied Sciences
European Centre for Living Technology (Venice, IT)
stdm@zhaw.ch

Christoph von der Malsburg

Frankfurt Institute for Advanced Studies
University of Zurich, ETH Zurich
malsburg@fias.uni-frankfurt.de

January 10, 2025

ABSTRACT

Nets, cooperative networks of neurons, have been proposed as format for the representation of sensory signals, as physical implementation of the Gestalt phenomenon and as solution to the neural binding problem, while the direct interaction between nets by structure-sensitive matching has been proposed as basis for object-global operations such as object detection. The nets are flexibly composed of overlapping net fragments, which are learned from statistical regularities of sensory input. We here present the cooperative network architecture (CNA), a concrete model that learns such net structure to represent input patterns and deals robustly with noise, deformation, and out-of-distribution data, thus laying the groundwork for a novel neural architecture.

Keywords net fragments · neural code · pattern recognition · computer vision · neural networks · cooperativity · neuroscience · machine learning

1 Introduction

Artificial intelligence (AI) systems have demonstrated remarkable capabilities in processing diverse types of data, including images, text, and speech (LeCun et al., 2015; Simmler et al., 2021). While many recent AI systems predominantly favor neural representations over symbolic ones, we follow a proposal by von der Malsburg et al. (2022) and present the *cooperative network architecture (CNA)*, an architecture that uses structured networks of mutually ('recurrently') connected neurons as representation of sensory signals. Using structured networks to encode information brings a diverse set of advantages, including high robustness, ability of figure reconstruction, and representing of out-of-domain data, laying the foundations to build novel object recognition frameworks (see Section 6).

The networks in the CNA are called nets and are dynamically assembled from overlapping net fragments, where net fragments are connectivity patterns that are learned by synaptic plasticity based on the statistics of sensory input signals. A major argument in favor of this data architecture is the possibility (as described repeatedly by Hinton (1981); von der

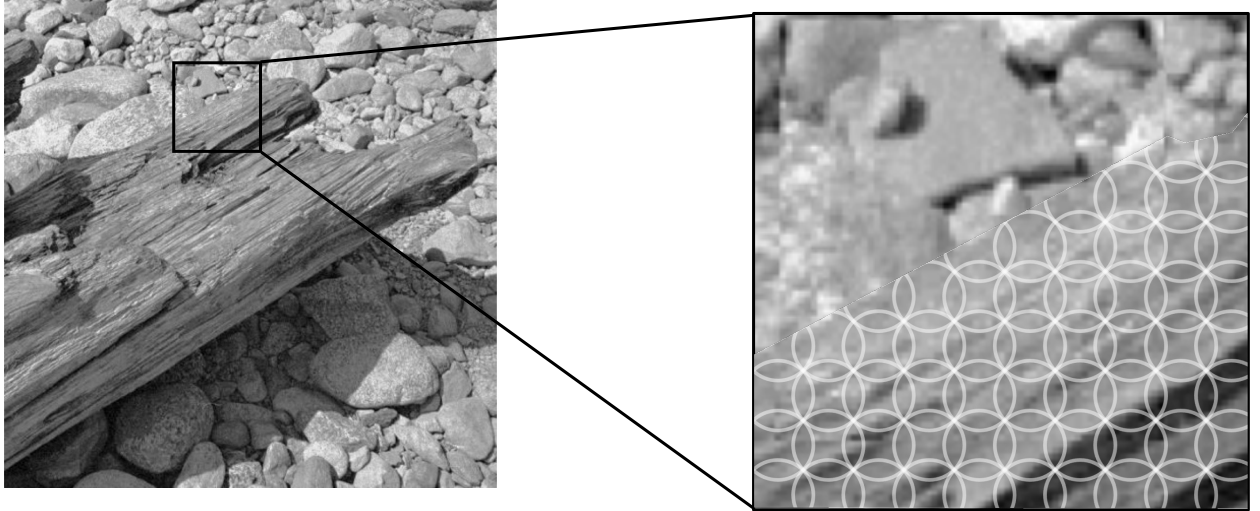


Figure 1: Representation of Objects by Nets. Objects are captured in their entirety by coherent nets that are composed of overlapping net fragments (schematically symbolized by white circles in the right panel). After training on natural images, each patch of visual space contains a complement of net fragments that represent textures that have been encountered with statistical significance. Net fragments overlap neuron-wise, and those activated by an object coalesce into a coherent net. The conundrum (stated in Olshausen and Field (2005)) that object contours can often not be found with the help of edge detectors due to lack of gray-level contrast (as in places inside the square in the left panel) may find its solution in that contours are defined as borders of the nets covering objects (or covering the background). Figure adapted from Olshausen and Field (2005), with permission.

Malsburg (1981); Anderson and Van Essen (1987); Kree and Zippelius (1988); Olshausen et al. (1995); Wiskott et al. (1997); Wolfrum et al. (2008); Memisevic and Hinton (2010); Arathorn et al. (2013)) of solving the invariant object recognition problem by structure-preserving mapping between nets representing variant images and invariant models of objects. The representation of image structure by recurrently connected nets formed between elementary feature detector neurons is a fundamental deviation from the current artificial neural networks (ANNs) paradigm, according to which image structure is represented by sets of complex-feature neurons activated by purely feedforward connections (see Section 2.3 for a comparison of the two approaches).

In the cited models of invariant object recognition, the formation of object-representing networks within the image domain (the primary cortical area where sensory signals arrive – here called ‘area’) has been sidestepped by letting spatial neighborhood stand in for connectedness. Neighborhood, however, is too weak a condition to qualify neurons as having responded to the same object (which is, for instance, apparent when looking at an object through foliage). Following von der Malsburg et al. (2022), we rather assume that for sets of neurons to be admitted into a net, they have to have been co-activated frequently in the past by structured visual input and consequently have been tied together by Hebbian synaptic plasticity (Hebb, 1949) into net fragments. Net fragments play a role somewhat related to the code-book vectors of some image compression schemes (Taubman and Marcellin, 2002) in representing statistically dominant texture patterns within any patch of the visual field; the formation of net fragments is somewhat related to, though fundamentally different from, associative memory (Hopfield, 1982), see Section 2.1.

CNA maintains that when a region of the area is hit by signals caused by an object, it transiently activates a subset of all the neurons in the area. The majority of those neurons are not part of a co-activated net fragment and have to be silenced. This is achieved with the help of some periodically rising inhibition, which silences those neurons and leaves active the small subset of all transiently activated neurons that are supporting each other by excitatory connections. Due to neuron-wise overlap, net fragments merge into a coherent net, which can span the entire region covered by an object’s image and thus connect feature neurons that are spatially distant through chains of locally connected intermediary neurons, see Figure 1. It is this *connectedness* that unites neurons activated by an object in forming a structured net that separates those neurons from the background and from occluding elements of other objects, thus solving the segmentation problem (von der Malsburg, 2024) and tying them into a network amenable to be mapped to an invariant model network in another cortical area (see the outlook in Section 6).

This study introduces the cooperative network architecture (CNA), representing the first concrete implementation of some fundamental components proposed in von der Malsburg et al. (2022). We focus on how to leverage networks as neural code and, specifically, discuss the

- establishment of a computational framework comparable to recent machine learning advances,
- learning of net fragments,
- demonstration of the activation of object-spanning networks (nets),
- demonstration of filter properties afforded by nets,
- discussion of nets in contrast to established ideas in neural computation and machine learning,

while relating to the significance of nets for invariant object recognition in multi-area settings only as outlook in the discussion section (i.e. we focus here on a single area while object recognition based on multiple areas is proposed for future research). We demonstrate that net fragments can be learned without relying on a teaching signal, whether supervised or unsupervised. This neural code exhibits robust capabilities for handling out-of-distribution data and effectively represents objects composed of fundamental features encountered during training—a task at which autoencoders (Hinton and Salakhutdinov, 2006) fail.

2 Relation to Alternative Concepts

The model we describe below is the first to demonstrate in concrete form the generation of structured nets that form a neural code to represent visual structure. To grasp the significance of the approach, it is important to compare it to alternative approaches.

2.1 Associative Memory

Associative memory (AM), as formulated by Amari (1972) or Hopfield (1982), shares with the present study the aim of retrieving previously encountered structure, and in both, the structure is recorded with the help of Hebbian synaptic plasticity. Whereas AM deals with the storage and retrieval of neural *firing patterns*, our purpose is to activate *networks*, that is, connectivity patterns that are structured by previously recorded connectivity pattern fragments. Admittedly, in both cases, the (re)construction process results in the activation of subsets of all neurons of the area, but whereas in AM, the connectivity of the set of active neurons is all-to-all, in our case, connectivity is restricted to within the net fragments that have previously been recorded, which in our visual application are restricted to short-range (local) connections and express two-dimensional topological structure. It is this structured connectivity that serves as basis for the structure-sensitive matching mentioned in the introduction. The monolithic all-to-all connectivity of the AM, by distinction, does not afford such structure-sensitive matching (i.e. instead of representing each structure as monolithic whole, the CNA learns to decompose them into local sub-patterns (net fragments), which can then be dynamically composed into nets to represent structures).

This functional difference is conditioned on a different mode of learning. Whereas in AM, a neural pattern is stored in a single event by strengthening the connections between any pair of currently active neurons, our approach distinguishes significant from insignificant connections, significant being those that are strengthened again and again, while insignificant are those that are strengthened only occasionally. This learning is driven by exposure to a large number of patterns, none of which may ever repeat, but which contain small repeating subpatterns. It is these that generate net fragments. In the visual case, it is local texture patches that play this role of repeating sub-patterns.

A basic limitation of AM is that unless the patterns to be stored are statistically independent (orthogonal), that is, have small neuron-wise overlap, they interfere with each other by the spurious activation of neurons. The problem can be reduced (as proposed by Tsodyks and Feigel'man (2007) or Palm (2013)) if patterns are sparse, that is, activate only a small fraction of all neurons. The statistical mode of pattern storage proposed here opens a more fundamental solution to the problem of pattern overlap. We propose that each input feature (specified by feature type and position) is represented not by one neuron but by a number of ‘alternative neurons’, neurons that have the exact same receptive field (for examples, see Cossell et al. (2015)), and thus are activated by the same afferents¹. While these neurons have the same afferent input, they can exhibit different excitatory output. Given this expansion, different net fragments with feature-wise overlap can reduce neuron-wise overlap by making use of different alternative neurons.

AM and our approach differ in yet another aspect, the mode of retrieval (or, in our case, construction) of patterns. In the version of Hopfield (1982) of AM, this is realized by minimizing an energy function by sequential switching of

¹There is ample space for alternative neurons, as there are 100 times more neurons in primary visual cortex than output neurons in the retina (Leuba and Kraftsik, 1994).

neurons. In our approach, winning patterns are projected out from the set of all neurons activated by the input and by rising inhibition that silences all those alternative neurons that do not have sufficient recurrent excitatory support, no neuron-sequential process being necessary.

2.2 Boltzmann Machine

Some important aspects of the system illustrated by our model are highlighted best by comparing it with the Boltzmann Machine (BM) proposed in Hinton and Sejnowski (1983). Both systems share features such as the ability to admitting recurrent connections (as does Mumford (2003)), but they also exhibit significant differences. Nevertheless, as our focus is limited to one area and is not the full architecture as proposed in von der Malsburg et al. (2022), we highlight only select differences here.

The BM makes a clear distinction between visible and hidden ('latent') neurons. In the CNA this distinction is softened: it posits neurons that are activated by sensory input, but of which the majority are quickly silenced by inhibition in favor of those neurons that support each other through previously learned connections. A winning alternative neuron can be interpreted as the hypothesis not only that the neuron has detected its trigger pattern in its afferents but also that the neuron has connections to a number of other active neurons and is consistent with them in light of previous experience.

In both BM and our model, the activity of hidden, or in our case alternative, neurons, is controlled by the same type of dynamic equations, with the difference that we do not insist on symmetric connections and therefore do not derive an energy function and consequently cannot prove convergence of the neural dynamics (see, however, the remark made in Hinton and Sejnowski (1983), that given sufficiently redundant support of active neurons, the missing of up to half of the connections due to lack of symmetry does not jeopardize stability of a state). In a single cycle of the periodically rising inhibition, convergence is not an issue, as alternative neurons undergo winner-take-all competition.

2.3 Artificial Neural Networks (ANN)

In the concept pursued here, objects and other structures within the input are represented by nets, sets of neurons that are held together by cooperative excitatory connections and are activated as a whole, the activation of individual neurons being conditioned on the activation of other neurons in the same net. In contrast, a large variety of ANN versions and learning techniques have been proposed, including multilayer perceptrons (MLPs) (Prince, 2023), transformers (Vaswani et al., 2017), autoencoders (Hinton and Salakhutdinov, 2006), or representation learning (Bengio et al., 2014). Common to all of these is that the sensory input is converted through many layers into a representation in the form of a set of neuron states. These neurons can be considered as propositions that indicate the presence of complex features (activity patterns) within the input. This representation of the input is then exploited by evaluation circuits (often in the form of a few fully connected layers of neurons) to achieve functions such as object classification, next-token prediction, or, in autoencoders, reconstruction of the input. The common feature of all ANN systems is that the connections from the input to the representation layer and from there to the output are purely feedforward and are trained by back-propagation of error (Rosenblatt, 1962, p. 292).

The CNA proposes a clear separation between input representation (within an area) and its functional evaluation (between areas, see Section 6). The representation of the input is trained by its statistics and is thus essentially neutral and without specialization to any specific function, giving it foundational character. In ANN systems, the selection of patterns to be extracted from the input is strongly biased to serve the trained function, which may be the reason that a transformer trained on one set of functions cannot continue to be trained on another (Dohare et al., 2024).

ANN's hierarchy of layers of neurons responding to features of intermediate complexity is replaced in the CNA by a single layer, in which net fragments of different sizes represent a hierarchy of features of varying complexity (and inter-mesh to form coherent nets standing for whole objects, thus solving the binding problem). The purpose of transition to other areas is, in the CNA, not transition to higher complexity but transition to representations that generalize over, e.g., position, size, or orientation of nets in lower areas, as discussed in Section 6.

In ANN systems, the high-level feature neurons that are activated by an input do not express any relations between them. This 'binding problem' (von der Malsburg, 1981; Burwick, 2014; Greff et al., 2020)) can give rise to ambiguity, e.g., the hallucination of feature conjunctions (Treisman and Schmidt, 1982). This ambiguity can be reduced by additional neurons whose trigger patterns overlap those of other neurons whose relative position would otherwise be in doubt (autoencoders (Hinton and Salakhutdinov, 2006) show that ambiguity can be suppressed altogether by a sufficiently large number of hidden neurons). In the CNA, the binding problem is solved in a natural way by net fragments that interconnect sets of features that co-occur with statistical significance in the input and that merge together into nets representing coherent chunks within a given input. This simplicity of representation of visual structure in CNA is due to its fundamentally different perspective on neural representation, in that the active state is not only described by

the elementary features that are active but also by the connections between them. This is made possible by different alternative neurons that represent the same elementary feature but express different connectivity.

3 Computational Framework

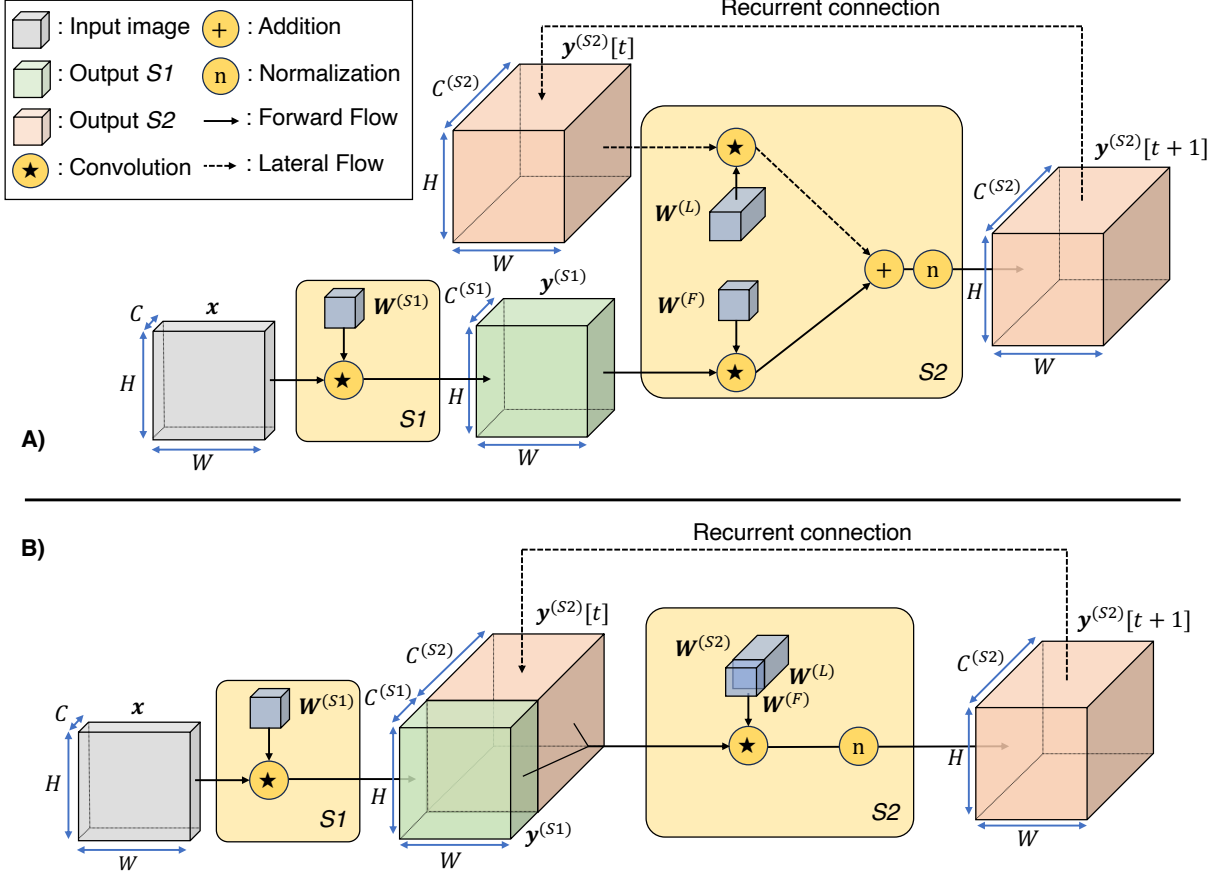


Figure 2: The dynamics of a single area within the proposed CNA: The input image is fed into stage $S1$ to obtain feature activations. The feature activations are then processed by stage $S2$, together with activations from neurons within the same layer. In part A, two distinct matrices are used to model the forward connections from $S1$ to $S2$ and the recurrent connections within $S2$. In part B, the matrices and input signals are concatenated, resulting in one bigger weight matrix.

Our framework addresses the visual system, even though it could be applied to other modalities as well. In the primary visual cortex, images appear as two-dimensional arrays of activated neurons, and its neurons are sensitive to local texture elements within their receptive fields (Grill-Spector and Malach, 2004). To account for the homogeneity of image structure, it can be assumed that the connectivity has translational symmetry ('convolutional' structure) supporting equivariance, that is, the property that image shift gets reflected in activity shift. We use these insights to build a CNA with two stages, as shown in Figure 2(A). The CNA is based on an input layer representing observed images by simple feature detectors and two layers, *Stage 1* (denoted as $S1$) and *Stage 2* (denoted as $S2$).

Feature Extraction. The system's input is a retinal 2D image represented by variables $\mathbf{x}_{k,i}$ (gray box in Figure 2), where $k \in (1, \dots, C)$ denotes the channel index of the image ($C = 1$ for grayscale, $C = 3$ for RGB), and the composite index $i = (h, w) \in (H \times W)$ stands for vertical and horizontal position of pixels within the input image.

Such an image is used as afferent input to the feature extraction neurons in $S1$ and first increases their 'membrane potential' $\mathbf{a}^{(S1)} \in \mathbb{R}^{C^{(S1)} \times H \times W}$ and potentially triggers their binary activation state $\mathbf{y}^{(S1)} \in \{0, 1\}^{C^{(S1)} \times H \times W}$ (green

box in Figure 2). The membrane potential $\mathbf{a}^{(S1)}$ is calculated by applying a convolutional operation (LeCun et al., 1989) (yellow box $S1$ in Figure 2):

$$\mathbf{a}_{c,j}^{(S1)} = \sum_{k \in C} \sum_{i \in l_j} \mathbf{W}_{c,k,j-i}^{(S1)} \cdot \mathbf{x}_{k,i} \quad (1)$$

Here, $c \in C^{(S1)}$ denotes the feature channel, the compound index j , expanded as $j = \{h, w\}$, designates again spatial position $h \in H$, $w \in W$, and the compound index $i = \{h, w\}$ is running through all (h, w) -pairs in the two-dimensional range $l_j = (h, \dots, h + h^{(W1)}; w, \dots, w + w^{(W1)})$ where $h^{(W1)}$, $w^{(W1)}$ denote the size of the convolutional filter. The size of the convolutional kernel used for feature extraction is $\mathbf{W}^{(S1)} \in \mathbb{R}^{C^{(S1)} \times C \times h^{(W1)} \times w^{(W1)}}$.

Feature Binarization. The membrane potential $\mathbf{a}^{(S1)}$, together with a bias parameter $b^{(S1)}$, determines the binary output of the neurons in $S1$, denoted as variable $\mathbf{y}_{c,j}^{(S1)} \in \{0, 1\}^{C^{(S1)} \times H \times W}$, where 1 stands for firing, 0 for silence. The binary neuron model with the input-output function $B : \mathbf{a}, b \rightarrow \mathbf{y}$ is defined as

$$\mathbf{y}_{c,j}^{(S1)} = B(\mathbf{a}_{c,j}^{(S1)} - b^{(S1)}) = \begin{cases} 1, & \text{if } \mathbf{a}_{c,j}^{(S1)} - b^{(S1)} > 0 \\ 0, & \text{otherwise} \end{cases} \quad (2)$$

with the same bias parameter $b^{(S1)}$ for all neurons acting as a firing threshold (neurons fire if the membrane potential is above this threshold).

Dynamics. Stage $S2$ builds net fragments by allowing active neurons to support recurrently connected neurons over T time steps (depicted as recurrent connection in Figure 2). A sample image is introduced into the system at time step $t = 0$ to activate neurons and remains unchanged until time step $t = T$. Throughout this period, neuronal activity undergoes sparsification due to growing inhibition (see below). Through the sparsification process, the system forms an object representation by leaving active a set of neurons each of which is supported by active neighbors, that is, a net.

Short-Range recurrent Connections. Although typical convolutional neural networks (Fukushima, 1980; Waibel et al., 1987; LeCun et al., 1989) apply convolution operations to establish *feedforward* connections between different layers, we employ them here to implement short-range *recurrent* connections within the same layer, their symmetry permitting a pattern to manifest itself at any spatial location based on corresponding net fragments. Given recurrent connections, the neural activity of the previous time step $t - 1$ is accessed to calculate a neuron's activity at time t . In contrast to recurrent networks like LSTMs (Hochreiter and Schmidhuber, 1997), where a new token is input at each time step, we iterate over the same input while updating the internal state to project out a net representing a given sensory signal. Importantly, the internal state evolves continuously, even when processing the same input pattern, driven by dynamic changes in the support between neurons along recurrent connections.

The membrane potentials $\mathbf{a}_{c,j}^{(S2)}$ of the second stage neurons get excited by the (constant) signals of the previous stage $S1$ and iteratively by recurrent excitation from within $S2$. Before digitization, they are modified by saturation, normalization, and inhibition (yellow box $S2$ in Figure 2). Before those modifications, its raw form is computed as:

$$\mathbf{a}'_{c,j}^{(S2)}[t] = \underbrace{\left(\sum_{k \in C^{(S1)}} \sum_{i \in l_j} \mathbf{W}_{c,k,j-i}^{(F)} \cdot \mathbf{y}_{k,i}^{(S1)} \right)}_{\text{Forward Connection}} + \overbrace{\left(\sum_{k \in C^{(S2)}} \sum_{i \in l_j} \mathbf{W}_{c,k,j-i}^{(L)} \cdot \mathbf{y}_{k,i}^{(S2)}[t-1] \right)}^{\text{Recurrent Connection}}. \quad (3)$$

Similar to $S1$, $c \in C^{(S2)}$ denotes the feature channel of $S2$, the compound index j expands to $j = \{w, h\}$, $w \in W$, $h \in H$, and the compound index i is running in the range $l_j = (h, \dots, h + h^{(W2)}; w, \dots, w + w^{(W2)})$, with $h^{(W2)}$ and $w^{(W2)}$ being the size of the convolution kernel.

The forward connections are denoted as $\mathbf{W}^{(F)} \in \mathbb{R}^{C^{(S2)} \times C^{(S1)} \times h^{(W2)} \times w^{(W2)}}$ and the recurrent connections as $\mathbf{W}^{(L)} \in \mathbb{R}^{C^{(S2)} \times C^{(S2)} \times h^{(W2)} \times w^{(W2)}}$, where $C^{(S2)}$ is the number of channels in $S2$, including the set of all feature channels and its alternative channels, i.e. $C^{(S2)} = n_a \cdot C^{(S1)}$ where n_a denotes the number of alternative channels per feature type (the alternative channels handle the alternative neurons that are required to prevent cross-talk between fragments). In the case of the forward connections, the kernel size determines which of the neurons $\mathbf{y}^{(S1)}$ in stage 1 can be connected

to a neuron $\mathbf{y}^{(S2)}$ in stage 2 (red box in Figure 2), while the kernel size of the recurrent connections determines which neurons can be connected within stage 2. The kernel $\mathbf{W}^{(F)}$ is initialized such that the sets of equivalent neurons in $S2$ copy the activity (and with that the feature type) of the corresponding neuron in $S1$, and $\mathbf{W}^{(L)}$ is initialized with zeros except for self-coupling of neurons, with value 1 (details in Appendix A). The weights are updated using Hebbian Learning (details in Appendix B).

For the first time step $t = 0$, when $\mathbf{y}_i^{(S2)}$ is undefined, we initialize the $S2$ neurons with zeros, i.e., the neurons are silent and do not provide recurrent support:

$$\mathbf{y}_i^{(S2)}[t = 0] = 0 \quad (4)$$

Single Weight-Kernel Implementation. This entire process is visually depicted in the upper part (A) of Figure 2. For simplicity in our algorithm, and since we use the same kernel size for the forward and recurrent connections, we stack the two kernels $\mathbf{W}^{(F)}$ and $\mathbf{W}^{(L)}$ as $\mathbf{W}^{(S2)} = (\mathbf{W}^{(F)}; \mathbf{W}^{(L)})$ as well as the inputs $\mathbf{y}_{k,i}^{(S1)}$ and $\mathbf{y}_{k,i}^{(S2)}[t - 1]$ as shown in Figure 2(B), leading to the equivalent formulation:

$$\mathbf{a}_{c,j}^{(S2)}[t] = \sum_{k \in C^{(S1)}} \sum_{i \in l_j} \mathbf{W}_{c,k,j-i}^{(S2)} \cdot (\mathbf{y}_{k,i}^{(S1)}; \mathbf{y}_{k,i}^{(S2)}[t - 1]) \quad (5)$$

The net fragments are implicitly contained in this processing as the active neurons whose activity state is stored in $\mathbf{y}^{(S1)}$ and their connection to other neurons.

Inhibition. The raw neural excitation \mathbf{a}' computed in eq. 3 (or eq. 5) is to be subjected to saturation, inhibition, and normalization so it can be binarized using a pre-defined threshold. These steps of processing the raw membrane potential \mathbf{a}' of neurons proved necessary in our simulation experiments to achieve the qualitative function we aimed for. The details to obtain the normalized activations \mathbf{a}^{norm} in the range $(0, 1)$ are described in Appendix C. The differences between activation levels of neurons are accentuated by setting

$$\mathbf{a}_{c,j}^{(S2)}[t] = \max \left(\left(\mathbf{a}_{c,j}^{\text{norm}}[t] \right)^\gamma, 0 \right), \quad (6)$$

The coefficient γ regulates the inhibition strength and increases with the time-steps of the inner loop according to $\gamma = 1.2 + 0.2t$, making it harder for neurons to fire (as $\mathbf{a}^{\text{norm}}[t] \leq 1$). The membrane potential is higher for neurons that are part of coherent fragments (valid patterns) as they receive recurrent support, while invalid activations are less supported. While the inhibition coefficient increases over time, many neurons eventually get suppressed, leaving only those active that support each other and form a consistent net. Finally, the membrane potential is converted to a binary activation, neurons becoming active when their inhibited membrane potential is above the activation bias $b^{(S2)}$, which serves to control the firing rate of neurons:

$$\mathbf{y}_{c,j}^{(S2)}[t] = B \left(\mathbf{a}_{c,j}^{(S2)}[t] - b^{(S2)} \right) \quad (7)$$

The final output $\mathbf{y}^{(S2)}[t = T]$ is the recurrent connection-supported neuronal activation in which, in contrast to the initial activation, unsupported activations are suppressed. Alternative neurons are connected by distinct channels within the convolutional matrix and engage in competition, with only one alternative channel gaining activation at each spatial location while the remaining neurons are suppressed (set to zero). This selection process is described in the Appendix D.

Relation to Nets and Fragments. Net fragments are *learned* through the strengthening of recurrent connections $\mathbf{W}^{(L)}$, facilitated by Hebbian plasticity. Neurons within a fragment are interconnected, providing mutual support that enhances their membrane potentials. By shifting $\mathbf{W}^{(L)}$ as convolutional kernels across the input, fragments can be detected at all spatial locations, resulting in numerous overlapping fragments. Coherent fragments are interconnected to form a larger structure, a net.

While multiple nets may exist, projecting out the most coherent one is crucial for robust object representation. This is achieved by progressively increasing inhibition over time. As inhibition intensifies, neurons with insufficient support (e.g., only a few instead of many neurons within one net fragment were triggered) are deactivated². This deactivation

²Neuron activations can be interpreted as hypotheses that require confirmation/support from other neurons with compatible hypotheses - otherwise, they are deactivated.

can propagate, leading to the elimination of entire fragments and leaving a single coherent net to represent the input structure.

In our experiments (see below), we observe that, initially, neurons operate independently due to the absence of established recurrent connections, with a single neuron having a membrane potential of 1 being sufficient for activation. However, after training, the average membrane potential rises to approximately 12, reflecting robust support from neurons within a fragment. As a result, inconsistent neurons can no longer activate (and neurons with a membrane potential of 1 are switched off), ensuring a more stable and coherent representation.

4 Experiments

To demonstrate the compositionality of net fragments, we train (updating $\mathbf{W}^{(L)}$ with Hebbian plasticity) the model on binary images containing straight-line patterns. For evaluation (after training and without updating any connections), we use images of kinked lines, digits, characters, and line drawings of objects such as houses and clocks. These complex patterns can be expressed as compositions of straight-line net fragments, even though the CNA was not explicitly trained on such patterns. This flexible compositional behavior contrasts strongly with associative memory (see Section 2.1). To highlight the differences between ANNs, we train and evaluate an autoencoder on the same dataset and compare the representations.

Besides compositionality, we introduce noise to examine the robustness and persistence of coherent structures with statistical relevance. Specifically, we assess the efficacy of filtering out random Gaussian noise and reconstructing partially occluded objects, i.e., the efficacy of dealing with subtractive noise. We introduce additive Gaussian noise to the afferent input in stage $S2$, thereby simulating an image structure that has already survived the filtering of feature kernels in $S1$ (thus increasing the difficulty, as the fragments must handle all the noise rather than relying on the feature extraction stage).

Further experimental details are provided in the Appendix: We describe the training and testing datasets in more detail in Appendix E, the feature extractor mechanism to obtain $\mathbf{y}^{(S1)}$ is described in Appendix F, the training details of our CNA model are in Appendix G, and the training details of the autoencoder in Appendix H.

5 Results

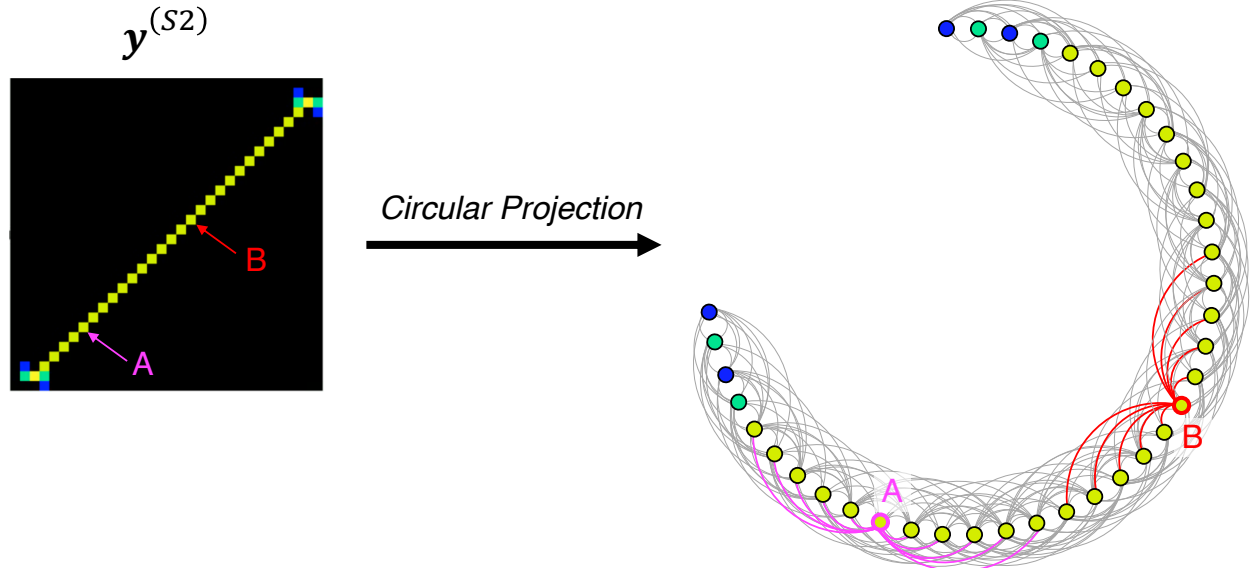


Figure 3: Net formed by activated neurons. The left of the image shows the neuronal activation $\mathbf{y}^{(S2)}$ when observing a line, and the right visualizes the net formed by these neurons. For convenience, the neurons are rearranged in a circle, and the connections of two randomly selected neurons, A and B, are visualized in colors (purple and red).

We empathize that this work focuses on learning a new neural code and, in the following, demonstrates it on a rather simple dataset.

Although our result figures display activated neurons, we would like to emphasize that these neurons are carriers of connections and form part of nets. To make this point for once, Figure 3 depicts this connectivity of activated neurons in $y^{(S2)}$ (arranged as a circle for convenience).

5.1 Compositionality

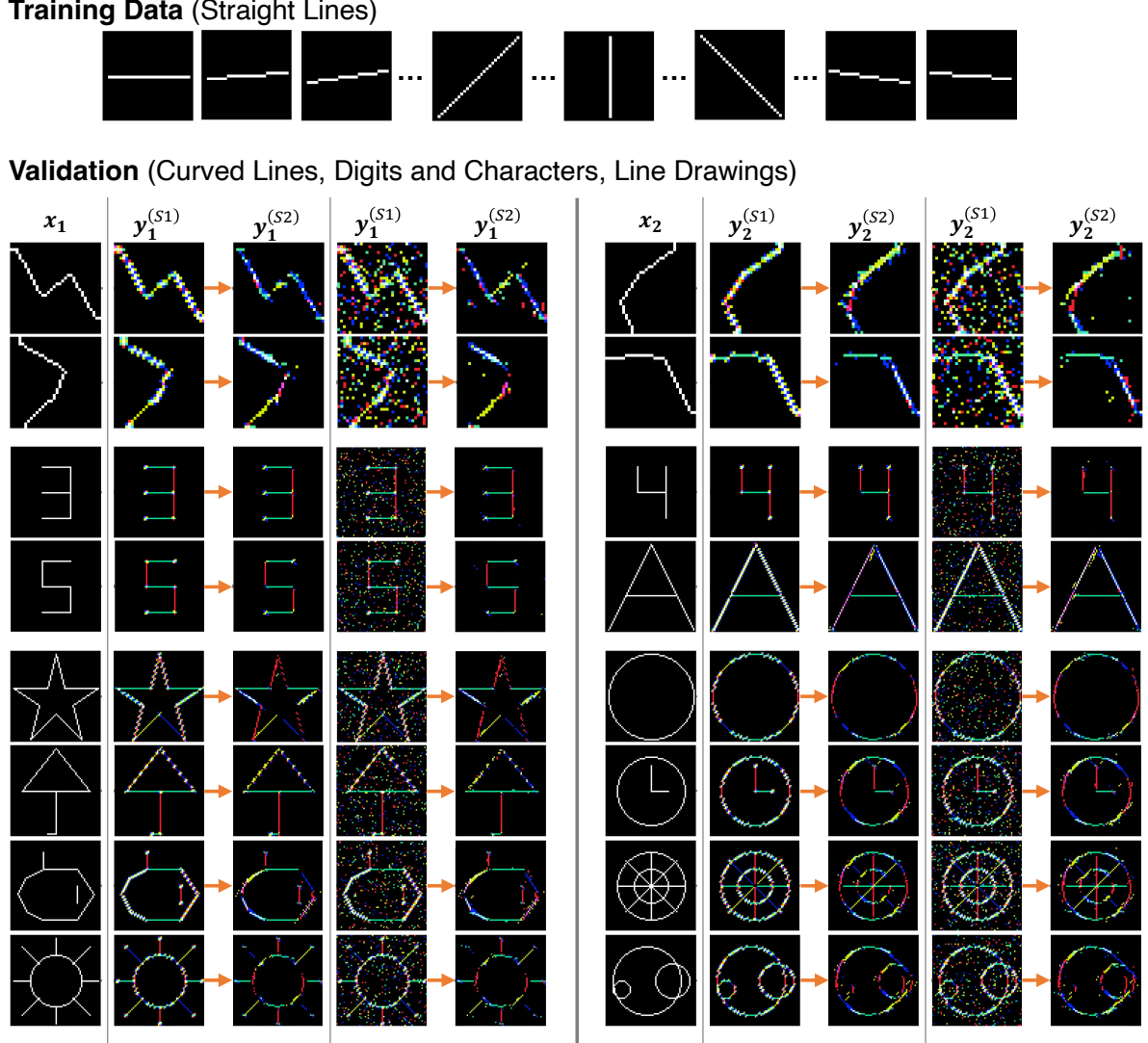


Figure 4: The top of the figure illustrates the straight lines used during the training phase. Below, various samples from the evaluation datasets are shown, including kinked lines (rows 1 and 2), digits and characters (rows 3 and 4), and line drawings (rows 5-8). For each row, two input examples, denoted as x_1 and x_2 , are displayed alongside their respective feature activations, $y^{(S1)}$, and neuronal activations, $y^{(S2)}$, shown both without and with addition of Gaussian noise.

The model weights, $\mathbf{W}^{(S2)}$, are trained using straight lines (see training data at the top of Figure 4), allowing the model to capture the underlying structure of straight lines within net fragments. The model composes these fragments dynamically into nets to represent much more complex structures (see validation data in rows 1-8 of Figure 4). For instance, despite not encountering these images during training, the CNA model can represent kinked lines (rows 1 and 2), digits and characters (rows 3 and 4), and line drawings (rows 5-8).

The motivation for why we build net fragments ($y^{(S2)}$) and not just use the feature activation $y^{(S1)}$ is demonstrated by introducing additional clutter: For each sample, we generate an input representation both with and without Gaussian noise. This noise corresponds to invalid patterns not observed during training, which lack sufficient recurrent support, leading to the deactivation of the corresponding neurons. Thus, the CNA model only allows valid sub-patterns to persist and be composed into novel structures, while invalid patterns, such as noise, are suppressed.

5.2 Filtering Gaussian Noise

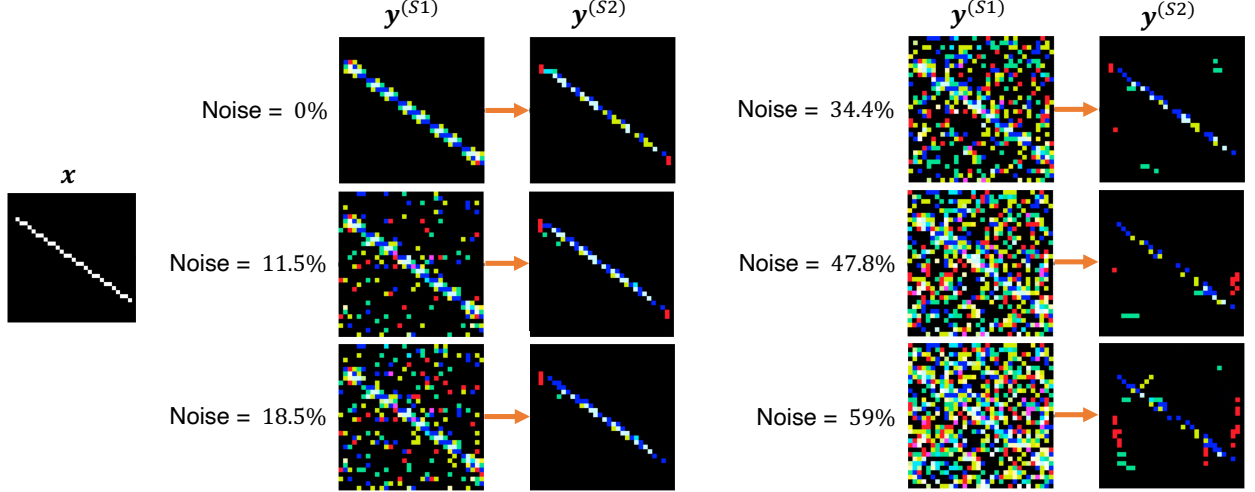


Figure 5: Noise-corrupted feature activations $y^{(S1)}$ alongside the corresponding output $y^{(S2)}$, in which noise is reduced due to suppression of neurons not supported by recurrent connections of net fragments. In each image, the background is shown in black, and the four different features in distinct colors. The plots are created using a bias $b^{(S2)} = 0.5$ and an inhibition coefficient $\gamma = 1.2 + 0.2t$.

The illustration in Figure 5 visually demonstrates the system's effective capability of filtering out isolated noise or small clusters thereof. Noise of varying degrees (from 0% to 59% noise at each spatial location - see Appendix E) is introduced in an area's afferent input, from which a significant portion is removed when constructing net fragments. While introducing up to 47.8% noise, remarkably consistent outputs $y^{(S2)}$ are generated. As additional noise is introduced, more undesired neurons receive support and persist in their activity. However, the overarching pattern remains distinguishable even when subjected to noise levels of up to 59%. In Appendix I, we quantitatively confirm the efficacy of noise filtering by measuring precision, recall, and noise filtration rate for various parameter settings, showing that lines remain well distinguishable for up to 59% added noise.

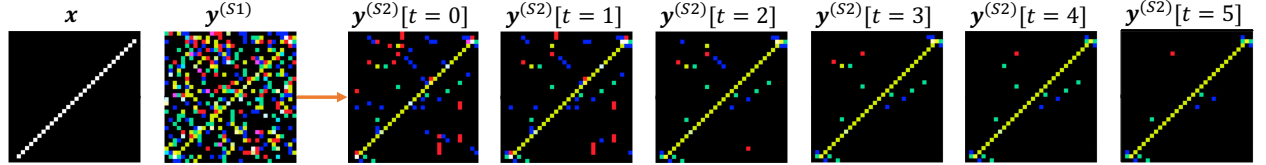


Figure 6: The filtering of (simulated) noise over time: Already at time step $t = 0$, most of the noise is suppressed. However, when inhibition increases over time, even more noise is filtered out in the course of iteration. The plot is created after adding 10% noise to each feature channel (sing a bias $b^{(S2)} = 0.7$ and an inhibition coefficient $\gamma = 1.2 + 0.2t$).

Figure 6 depicts this systematic filtering over time. The additionally introduced clutter doesn't activate overlapping net fragments and cannot persist over time. The figure illustrates a substantial noise reduction already at time step $t = 0$ due to the filtering by matrix $W^{(F)}$ and initial inhibition. In each subsequent time step, additional clutter is removed. This reduction is due to increased inhibition and falling support as a consequence of the drop-out of supporting neurons, demonstrating how overlapping fragments build a coherent net of mutually supporting neurons.

5.3 Reconstructing Figures

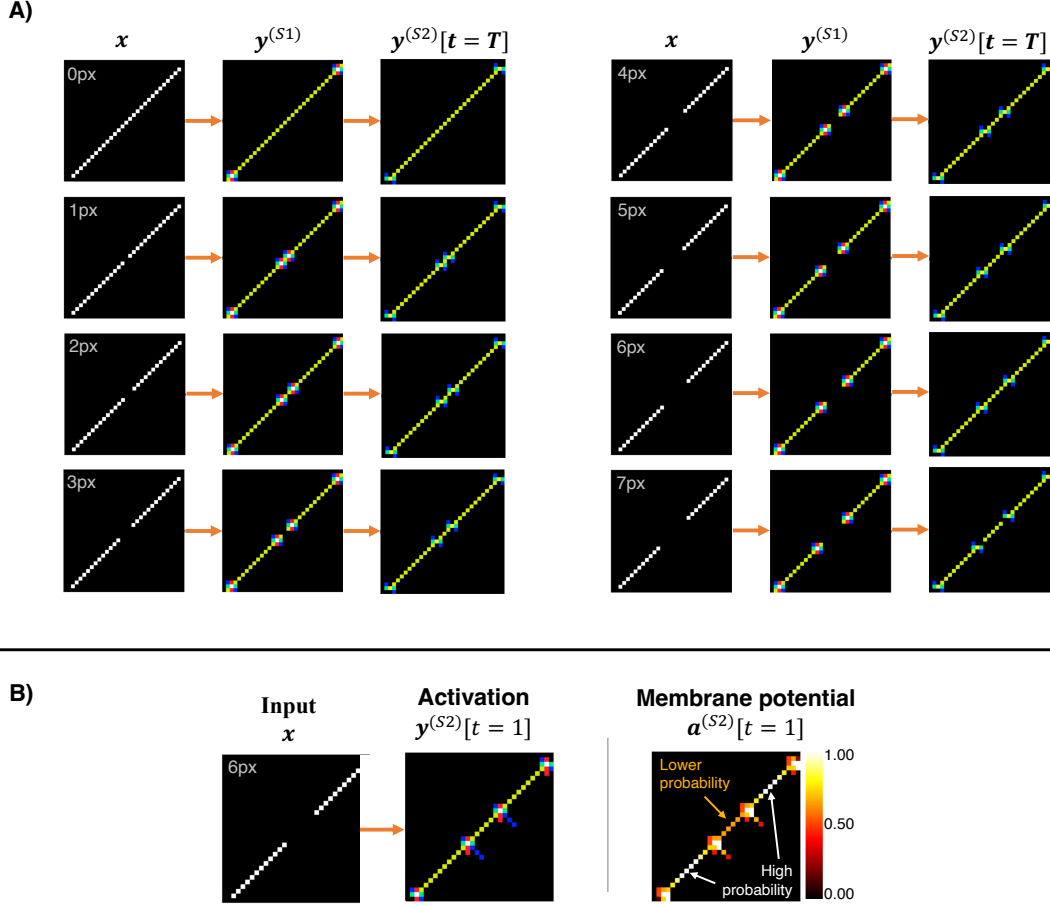


Figure 7: **Part A:** Input images of diagonal lines with different numbers of missing pixels, denoted in the top left corner of the panels (left column), corresponding feature activations (middle column), and final output neuron activations. Activation bias $b^{(S2)} = 0.5$, inhibition coefficient $\gamma = 0.6 + 0.2t$. **Part B:** Diagonal line with 6 missing pixels in the center (shown on the left), the corresponding output activity (in the middle), and the membrane potential $a^{(S2)}$ displaying the ‘activation probabilities’ (on the right) after the first time step.

If a substantial number of neurons activate and support other neurons within a net, inactive neurons can receive significant support, leading them to switch on and encouraging figure reconstruction. Figure 7A shows how inactive neurons activate and thus demonstrates that nets can deal with occluded patterns. This reconstruction works only reliably for up to 3 missing pixels (see Appendix I). In some cases, as in this Figure, the line is fully reconstructed for up to 6 removed pixels and partly reconstructed for 7 pixels.

Membrane Potential Represents Expected Feature Activation. When dealing with missing pattern elements, the membrane potential map $a^{(S2)}$ is higher at spatial locations where line features are observed and lower where they are not observed but expected. Consequently, the network can, to some extent, handle this ambiguity and model it based on the activation map, as shown in Figure 7B. Modeling this ambiguity enables having different internal interpretations, such as whether ‘it is an interrupted line that should be reconstructed’ or ‘there are two co-linear line segments’ and selecting one of them based on the threshold $b^{(S2)}$.

Increasing Inhibition Over Time Stabilizes Patterns. The reconstruction process unfolds across multiple sequential steps, as illustrated in Figure 8. Initially, at time step $t = 0$, the net fragments represent the interrupted line. Subsequently, during the second time step ($t = 1$), one of the removed pixels is reconstructed, and shortly after, at $t = 2$, the entire line is represented. Thus, reconstruction can persist even amid increasing inhibition, given that inactive neurons receive

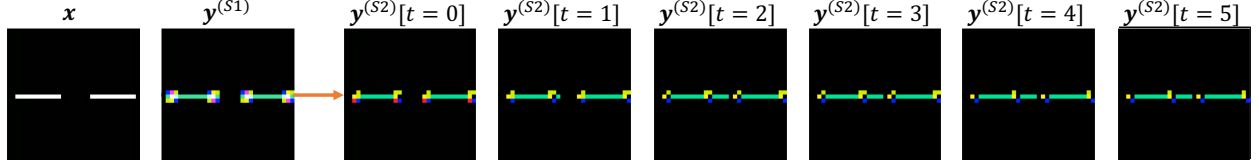
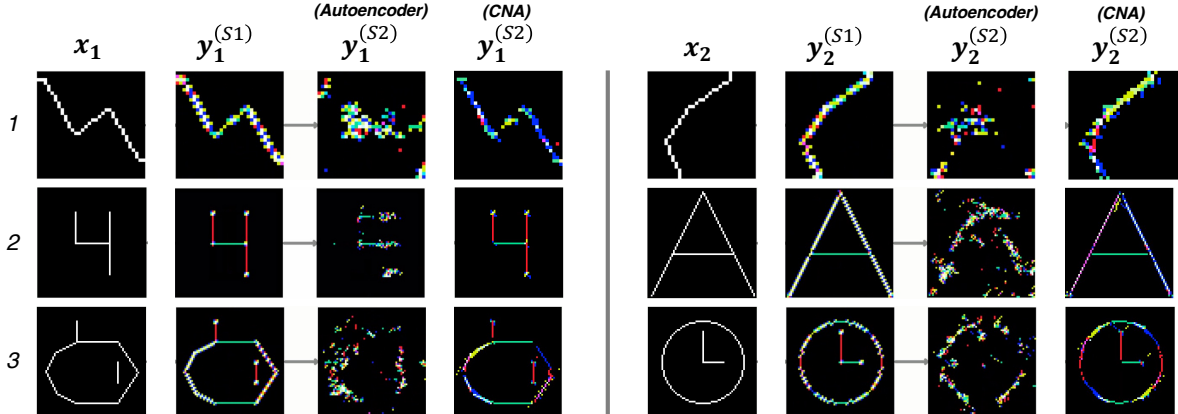


Figure 8: Reconstruction of a horizontal line interrupted by 7 pixels: The feature activation and the initial output activity at $t = 0$ are interrupted but reconstructed within the two subsequent time steps ($t = 1, 2$). Afterward, some artifacts triggered at line ends are reduced due to increasing inhibition. Activation bias $b^{(S2)} = 0.5$, inhibition coefficient $\gamma = 1.8 + 0.1t$.

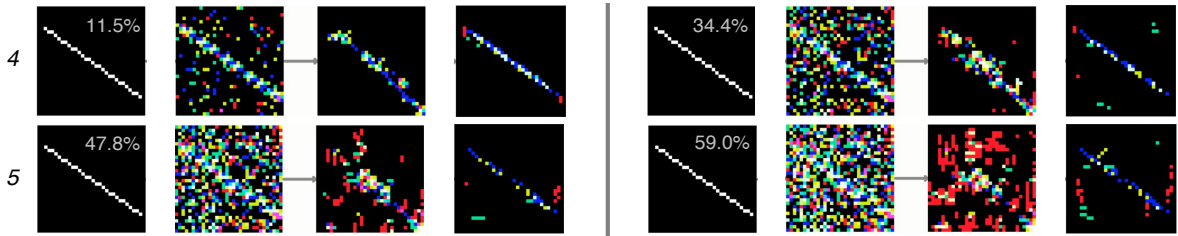
adequate support. This example underscores the necessity for multiple time steps, essential not only for noise removal but also for the reconstruction of features, as neurons can undergo flipping in each time step, fostering a dynamic interplay where the flipping of neurons encourages others to follow.

5.4 Comparison to an Autoencoder

Compositionality



Noise Removal (ratio of noise shown in top right of input data)



Line Reconstruction (number of removed pixels in top left of input data)

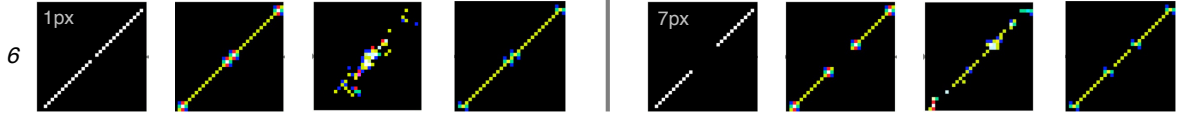


Figure 9: Comparison of the outputs generated by the proposed CNA model and an autoencoder across different tasks. Each row presents two samples, x_1 and x_2 , alongside their respective feature activations and resulting representations (once for the CNA model and once for the autoencoder). Rows 1 to 3 illustrate how both models encode patterns that were not present in the training dataset. Rows 4 and 5 compare the models' performance in denoising tasks, while row 6 evaluates their ability to reconstruct lines.

Figure 9 compares performance between the proposed CNA model and an autoencoder (for model details, refer to Appendix H). While the autoencoder successfully learns to accurately represent line structures in the training data - achieving a mean square error (MSE) of less than 1×10^{-3} between the input and decoder reconstruction - it struggles with generalization to data not observed during training. For instance, rows 1 to 3 demonstrate that the CNA model is capable of representing previously unseen structures, while, in contrast, the autoencoder fails to capture such out-of-distribution patterns.

Rows 4 and 5 highlight the autoencoder's ability to represent line structures with up to 11.5% noise introduced. However, as the noise level increases, its performance decreases significantly. The CNA model, by contrast, remains robust under much higher noise levels, tolerating up to 59% noise while still producing high-quality representations. Metrics on noise reduction, precision, and recall, presented in Appendix I, further substantiate the CNA model's superior performance.

In row 6, the models' capabilities in reconstructing missing line segments are compared. Both models can reconstruct the removed pixels, but the autoencoder introduces additional noise in regions other than the line center, where the pixels were removed. This is confirmed by the metrics in Appendix I: The autoencoder is slightly superior in reconstructing the removed pixels, but this comes at the cost of more noise at other locations, leading to lower overall precision and recall.

6 Discussion and Outlook

The CNA presented here establishes a novel approach to construct coherent nets as neural representations of visual input, enabling arrays of elements to be treated as unified gestalts through the composability of previously learned sub-patterns (net fragments). While the concept of such net construction has been proposed theoretically (von der Malsburg et al., 2022), this work marks the first successful implementation and simulation of the idea.

Our approach offers distinct advantages over existing neural coding frameworks, particularly in terms of robustness and the ability to represent out-of-domain data. Using nets of neurons to represent sensory signals allows filtering out noise and figure completion, while using net fragments allows representing unseen objects through composing small feature patches. In contrast to past work that relied on manually constructed filter functions (e.g., Geman and Geman, 1984), the filter functions, nets in our scheme, are learned from input statistics resp. constructed on the spot, so that they will eventually be able to cover the whole gamut of patterns encountered in natural images.

An essential next step would be the construction of a system that is trained on natural images, that contains at each position of the visual field a complement of elementary feature detector neurons able to accurately represent the pixels of the input (as in Olshausen and Field, 1996), and whose recurrent connections have sufficient lateral extent to capture the most important signal correlations present in natural images. Such systems can then be expected to develop net fragments that capture and represent all textures encountered in natural images on that length scale, thus realizing the ambition expressed in Figure 1.

A first and important such operation is abstracting over position, size, and in-plane orientation of an object's image in the input area (primary visual cortex) by the construction of an invariant net representation of the object in a separate area (which would correspond to inferotemporal cortex (Ito et al., 1995)). As hinted at in the Introduction, this can be based on structure-sensitive, 'homeomorphic', mappings, as proposed in von der Malsburg (1981); Anderson and Van Essen (1987); Olshausen et al. (1995); Wiskott et al. (1997); Wolfrum et al. (2008); Memisevic and Hinton (2010) or Arathorn et al. (2013). A mapping is homeomorphic if it preserves neural feature type as well as connectivity. Object classification or recognition of individual objects can then be based on a further homeomorphic mapping to an area containing a more permanent schematic representation of the object class or a sample of the object to be recognized, as realized in Wolfrum et al. (2008).

The introduction of nets as a neural code and the inclusion of alternative neurons suggest a natural basis for the mapping process by requiring inter-areal connections to be not only specific to feature type but also to alternative neuron identity. As this identity contains information on net connectivity, this specificity can implement the homeomorphy constraint of inter-areal mappings in a natural way and overcome the limitations in existing systems (Wolfrum et al., 2008).

Once the mechanism of homeomorphic mapping has been established, it is available for arbitrary novel objects, thus forming the basis for invariant object recognition at first sight (as observed in humans in Biederman and Cooper (1991)). This capability stands in stark contrast to current ANN technology, which requires invariance to be trained individually for each object, highlighting the broader generalization potential of our approach.

The simple mechanism of net formation that we model here is a first but significant step in the direction of a data architecture grounded in nets connecting sparse sets of neurons within and between areas. Nets are singled out by the properties of cooperativity and inner consistency: all neurons of an active net experience the high-order coincidence

of converging excitatory signals, realizing predictive coding at each neuron. Given high sparsity of neural firing and high sparsity of connectivity, satisfying the requirement of consistency is highly non-trivial and can only be established by a learning process in which single neurons acquire converging connections coming from sets of neurons that fire simultaneously again and again, as realized in our model.

In summary, the CNA demonstrates the feasibility and potential of a principled and compositional approach to neural coding. Its ability to autonomously construct robust representations, handle out-of-domain data, and generalize to novel stimuli underscores its promise as a foundation for more advanced systems in the future, especially when extended with multiple areas.

Funding

This research has been funded by the Canton of Zurich, Switzerland, through the Digitalization Initiative of the Canton of Zurich (DIZH) Fellowship project ‘Stability of self-organizing net fragments as inductive bias for next-generation deep learning.’

Data Availability Statement

The code to generate the data as well as to reproduce the results can be found after the publication of this work on Github at <https://github.com/sagerpascal/cna>.

Appendix

A Weight Initialization

The forward connections $\mathbf{W}^{(F)}$ are initialized so that the activations of the $S1$ neurons are copied into the $S2$ neurons in the same position. This is done by setting the connections at the center of the kernel (at position $(h^{(W2)}/2, w^{(W2)}/2)$) to 1 if $c_{in} = \lceil c_{out}/n_a \rceil$, where c_{in} denotes the index of the input channel, c_{out} the index of the output channel, and n_a the number of alternative neurons.

The recurrent connections $\mathbf{W}^{(L)}$ are initialized with zeros except for the self-coupling of neurons, which is set to 1. When Hebbian plasticity is employed on the weight matrix $\mathbf{W}^{(L)}$, these connections ought to grow (as neurons tend to keep their activation state between time steps), but due to the constraint of keeping all connection weights within the range $(0, 1)$ (refer to equation 8), they stay put at 1.

B Hebbian Plasticity

After processing for T time steps both matrices $\mathbf{W}^{(F)}$ and $\mathbf{W}^{(L)}$ undergo Hebbian updates (Hebb, 1949):

$$\mathbf{W}^{(S2)} := \min \left(\max \left(\mathbf{W}^{(S2)} + \alpha \cdot \rho_{avg}, 0 \right), 1 \right) \quad (8)$$

where α represents the learning rate. Note that the network employs shared connections, formulated as convolutional kernels, between input patches and output neurons, making the building of fragments translation equivariant. Consequently, the same recurrent connection is applied across multiple output and input neurons. The decision to update this connection is based on the average correlation ρ_{avg} between all input and output neurons it connects. If the resulting average is positive, the corresponding connection increases by α as it connects more simultaneously active neurons than neurons that fire disjointly. Conversely, if the average correlation is negative, indicating more disjoint firing, the connection strength is reduced by α .

The actual modification eq. (8) is applied once after the last iteration over T timesteps to increase stability against fluctuation of the activities $\mathbf{y}^{(S2)}[t]$ in the course of iterations.

C Normalization

We use two normalization steps to confine the neuronal activations $\mathbf{a}'^{(S2)}$ to the interval $(0, 1)$.

We first apply a size limit:

$$\mathbf{a}'^{(S2)}_j[t] = \begin{cases} \mathbf{a}'^{(S2)}_j[t], & \text{if } \mathbf{a}'^{(S2)}_j[t] \leq \lambda \\ \lambda - \frac{1}{2}(\mathbf{a}'^{(S2)}_j[t] - \lambda), & \text{otherwise.} \end{cases} \quad (9)$$

According to this formula, \mathbf{a}' grows undiminished with \mathbf{a}' until it reaches the value λ , and thereafter actually diminishes with slope $-1/2$. (In our experiments we found the value $\lambda = 1.3 \cdot \frac{h^{(W2)} + w^{(W2)}}{2}$ to work well). This saturation helps to mitigate imbalances between net fragments with differing numbers of participating neurons. In the next step, we introduce the normalization

$$\mathbf{a}_{c,i}^{\text{norm}(S2)}[t] = \frac{\mathbf{a}_{c,i}'^{(S2)}[t]}{\max_{i'} \mathbf{a}_{c,i'}'^{(S2)}[t]} \quad (10)$$

This normalization confines activations to the interval $(0, 1)$, where neurons receiving maximal support are mapped to 1, while those with lesser support are mapped to correspondingly smaller values. This normalization relative to the maximal value that itself is growing during learning as it is important to give neurons initially (when recurrent connections are still small) a chance to fire and later, when recurrent links of often co-active neurons have grown, to suppress those neurons that are part of accidental or noise patterns.

D Alternative Neuron Selection

Only one of a set of alternative neurons is allowed to be active. The selection process is determined by evaluating the correlation between feature patches and alternative kernel filters. Initially, patches matching the size of the feature kernel are extracted from every position in the input $(\mathbf{y}^{(S1)}; \mathbf{y}^{(S2)}[t-1])$. Subsequently, the correlation of these patches with the feature kernels is computed, and at each location, the alternative kernel exhibiting the highest correlation is chosen. Consequently, multiple features may be active at each location, but only one of the competing feature channels — the one best matching a given input patch — achieves activation. At initialization (see Appendix A), where all alternative channels fit equally well to a given local pattern, the first channel is selected. However, after applying a Hebbian update, this channel starts specializing in recognizing a specific local pattern. Consequently, the activation of subsequent local patterns may either trigger the same channel if they have a high correlation or activate another channel better suited to recognizing the new pattern.

E Dataset

The dataset comprises binary images measuring (32×32) pixels, each sample depicting a straight line going through the image center, starting and ending 2 pixels from the image boundary (leading to 59 distinct lines of different angles).

The images are generated when required and may vary from one epoch to another. During each training cycle, we randomly generate 300 image instances (each line about 5 times). During evaluation, we sample each of the 59 distinct lines exactly once. In contrast to training, the samples used for evaluation comprise local distortions in the form of additive Gaussian noise and missing line segments (subtractive noise), and we evaluate the net fragments' capability to remove these.

To introduce additive Gaussian noise to the afferent input in stage $S2$, we probabilistically flip neurons within each channel with a probability of up to 20%. Since we use four feature channels in our experiments, this corresponds to a probability of $1 - (1 - 0.2)^4 = 59\%$ that a neuron is flipped at any spatial location. To evaluate subtractive noise, we create discontinuous lines by deleting a line segment of 1 to 7 pixels in the middle.

To demonstrate the generalization capability of CNA areas, we generate validation samples that differ from the ones used during training. Specifically, we produce binary images measuring (32×32) pixels depicting kinked lines by generating four random points within the image and drawing straight lines between these points.

Additionally, we generate binary images measuring (64×64) pixels by hand that represent more complex structures. These images include line drawings of digits 0-9, characters, and objects such as a house, a star, a wheel, a clock, etc. Some of these images are shown in Figure 4, and an extensive list can be found at <https://github.com/sagerpascal/cna>.

F Feature Extraction

The input images have $C = 1$ channel and $C^{(S1)} = 4$ features are extracted at each spatial location. We utilize hand-crafted filters with a size of 5×5 as displayed in Figure 10, each of the four filters corresponding to a particular

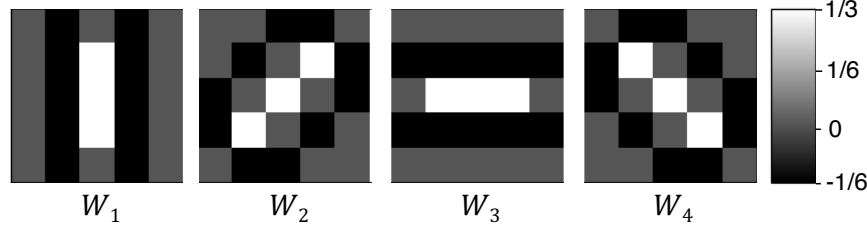


Figure 10: The hand-crafted convolutional kernels of the feature extractor.

line orientation (vertical, positive diagonal, horizontal, and negative diagonal). This approach is motivated by the observation that, given our specific elementary feature types (cf. Figure 10), straight lines, when viewed locally, can be expressed as combinations of these fundamental line types (e.g., a line with a 20° angle activates the horizontal and the $+45^\circ$ diagonal feature neurons). The use of such manually designed filters allows a more straightforward interpretation of the results. While more complex datasets necessitate learned filters, our primary focus in this work is on constructing net fragments, and thus, we favor the simplicity of hand-crafted filters.

These filters move across the image with a step size ('stride') of 1 (assuming 0 as input signal beyond the image border: 'zero padding') so that the input image and output image are of the same size. Thus, the input \mathbf{x} in the feature extraction stage are images of size $(1 \times 32 \times 32)$ and the output $\mathbf{y}^{(S1)}$ feature activation maps of size $(4 \times 32 \times 32)$. The dataset's lines activate multiple filters at different positions, facilitating the construction of net fragments across these feature channels. We convert the floating-point output of the convolutional weights to binary activations using binary neurons $B()$ with a bias of $b^{(S1)} = 0.5$, i.e. neurons fire a binary spike if $a_j > 0.5$ (see eq. 2).

G Parameters

We train the model with a learning rate of $\alpha = 0.2$ for 100 training cycles (epochs). The model uses $n_a = 10$ alternative neurons with recurrent connections spanning a kernel of 11×11 neurons. Since we use $C^{(S1)} = 4$ filters for feature extraction in $S1$ (see Appendix F), the number of alternative channels in $S2$ corresponds to $C^{(S2)} = 4 \cdot n_a = 40$. The resulting weight matrices have dimensions $\mathbf{W}^{(F)} \in \mathbb{R}^{40 \times 4 \times 11 \times 11}$ and $\mathbf{W}^{(L)} \in \mathbb{R}^{40 \times 40 \times 11 \times 11}$, respectively $\mathbf{W}^{(S2)} \in \mathbb{R}^{40 \times 44 \times 11 \times 11}$.

H Autoencoder Parameter

We compare our CNA model to an ANN, specifically an autoencoder (Hinton and Salakhutdinov, 2006), which is a widely used self-supervised technique for generating input representations. An autoencoder is particularly suited for comparison because it includes a built-in decoder, allowing for feature reconstruction and visualization, which is required for feature comparison. To ensure a fair comparison, we also employ convolutional filters (LeCun et al., 1989) to the autoencoder and incorporate state-of-the-art design principles (we even permit more data and feature channels to the autoencoder).

The autoencoder is trained to reconstruct the feature activations, $\mathbf{y}^{(S1)}$, using the same training dataset as our CNA model. It consists of an 8-layer architecture, with an encoder composed of convolutional layers with a kernel size of 3 and a stride of 2, with progressively increasing channel counts of 32, 64, 128, and 256 layers. The decoder mirrors this structure, using transposed convolutional layers with 256, 128, 64, and 32 channels, respectively. ReLU activations are applied after each layer. Consequently, the autoencoder is a relatively large model with 777k parameters, utilizing up to 256 channels, whereas the CNA model operates with only 44 channels.

The autoencoder is trained by minimizing the L2 norm between the input features and their reconstructed counterparts, using the Adam optimizer (Kingma and Ba, 2015) with a learning rate of 1×10^{-4} , beta parameters of $(0.9, 0.999)$, and a weight decay of 1×10^{-8} .

To provide a robust comparison, we increase the number of training samples for the autoencoder. Rather than training for 100 epochs with 300 samples per epoch as done for the CNA model, we train the autoencoder for 200 epochs, using 10,000 images per epoch. This results in a significantly larger training set but ensures that the autoencoder achieves a highly accurate reconstruction. The autoencoder is trained with a batch size of 512.

I Quantifying Noise Filtration

Our evaluations focus on the efficacy of net fragments in suppressing added Gaussian noise and complementing missing or occluded patterns. For both evaluation experiments, we report *recall* and *precision*: Recall is defined as the proportion of neurons that maintain activity (on) when noise is added, and precision quantifies the extent to which neurons activated in the presence of noise were also active without noise. To assess the system's noise reduction capability in the case of Gaussian noise, we additionally measure the percentage of flipped neurons that revert to their original activation state, referring to this measurement as the *noise reduction rate*. To assess subtractive noise, we measure the similarity between the original (created without noise) and reconstructed (created with noise) feature activations at the spatial locations where pixels have been removed. We call this metric the *feature reconstruction rate*.

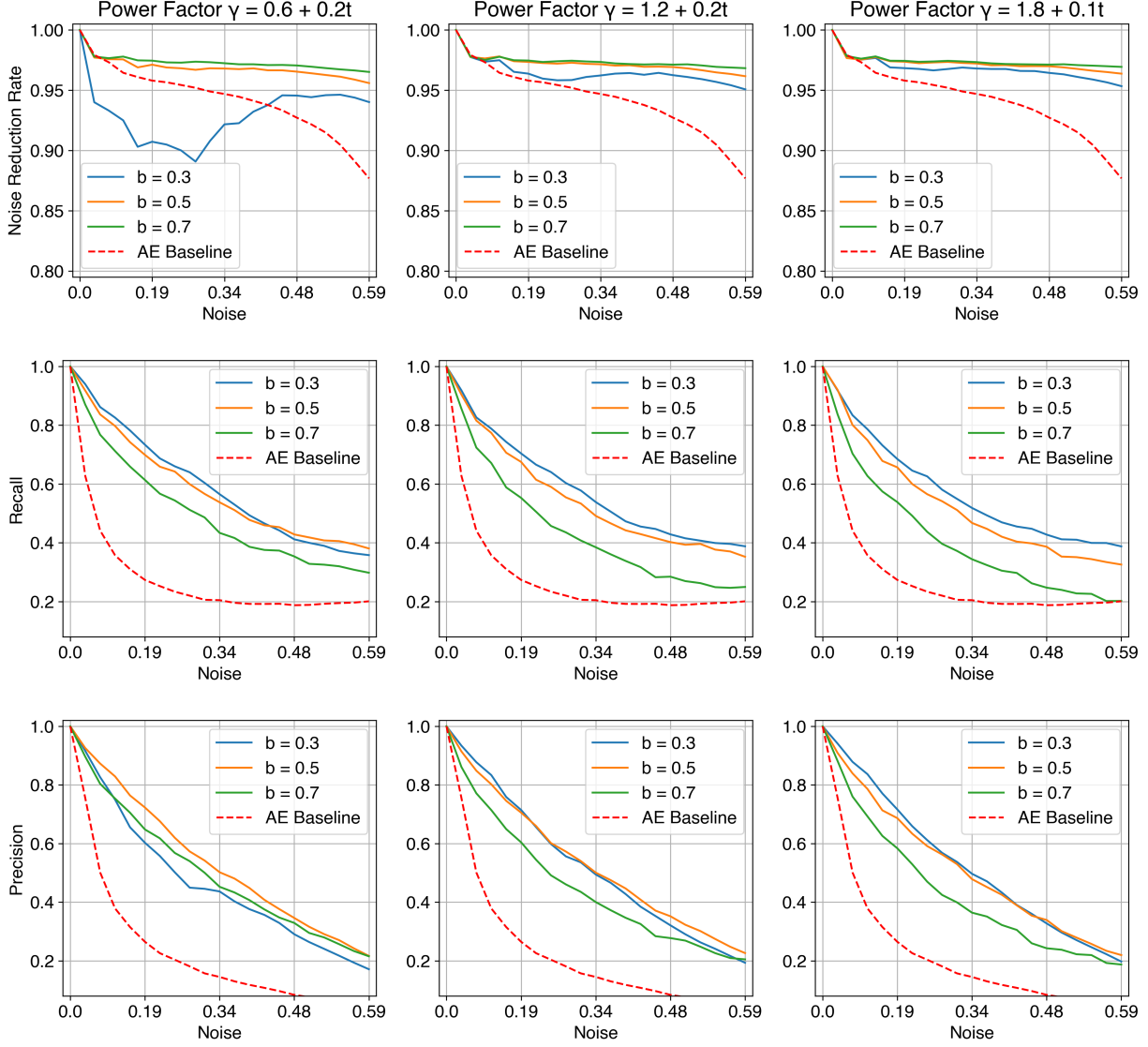


Figure 11: System performance as function of the noise level. First row: noise reduction rate; second row: recall; third row: precision. Columns differ in the inhibition coefficient γ that models inhibition. The colors within each plot represent different activation biases $b^{(S2)}$. The dotted red line is the autoencoder, serving as baseline.

Filtering Gaussian Noise. Figure 11 displays noise reduction rates, recall, and precision across different parameter configurations for different levels of added noise. The metrics demonstrate that increasing the inhibition coefficient or the activation bias results in enhanced noise filtration.

The overall efficacy of noise reduction remains consistently high across most parameter configurations, exhibiting a constant noise reduction rate of $\geq \approx 95\%$. This rate persists regardless of the magnitude of the introduced noise. As the noise suppression rate is approximately constant, this means that if there is more noise in the input, there will also be more noise in the output, albeit limited to around 5% of the input noise.

Furthermore, all CNA models (except the one with the lowest power factor and bias) outperform the autoencoder, demonstrating that they achieve performance that is competitive with state-of-the-art deep learning models.

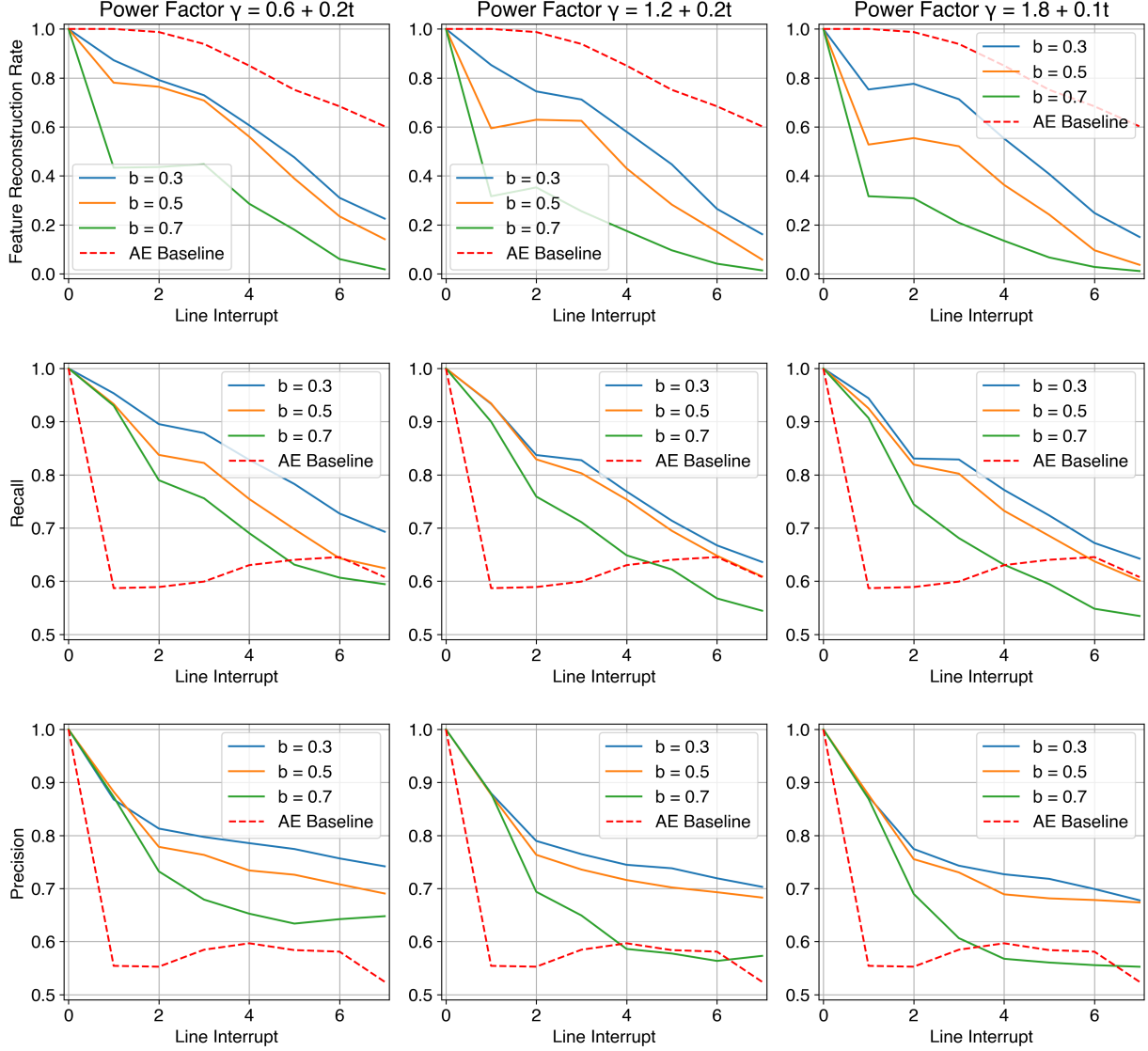


Figure 12: Reconstruction of partial occlusion. *First row:* feature reconstruction rate; *second row:* recall; *third row:* precision. Columns are distinguished by the inhibition coefficient γ , and line colors within plots distinguish activation bias $b^{(S2)}$. The dotted red line is the autoencoder model.

Reconstructing Subtractive Noise. Figure 12 displays the feature reconstruction rate, precision, and recall for removed line fragments of different lengths. Having a lower activation bias or inhibition coefficient γ leads to a better reconstruction of removed patterns, as these settings allow neurons with less support to activate.

Compared to the autoencoder baseline, the CNA model achieves higher recall and precision but a lower feature reconstruction rate. This indicates that the autoencoder is superior at reconstructing the pixels that have been removed but that, in general, much more noise (other neurons are activated/deactivated) is introduced.

Interpreting Metrics. While the reported values for precision and recall may appear low, we argue that these fragments are of good quality and point out that precision and recall metrics have to be interpreted differently than in a classification context: A net fragment consisting of many neurons characterizes (a part of) an object and maintains this characterization even when many of its neurons are inverted (and precision and recall are low). This aligns with the findings of Ahmad and Hawkins (2015), highlighting that binary distributed activations demonstrate high robustness, retaining accurate interpretation even in the presence of numerous flipped neurons.

In the case of the depicted straight lines, the feature neuron activations of the two most similar lines overlap with 21.2%. Therefore, achieving precision and recall values surpassing this threshold permits reliable discrimination even among similar lines, which is the case for the CNA but not for the autoencoder (e.g., see Figure 11).

References

- Ahmad, S. and Hawkins, J. (2015). Properties of Sparse Distributed Representations and their Application to Hierarchical Temporal Memory. *arXiv*, (preprint arXiv:1503.07469).
- Amari, S.-I. (1972). Learning patterns and pattern sequences by self-organizing nets of threshold elements. *IEEE Transactions on Computers*, C-21(11):1197–1206.
- Anderson, C. and Van Essen, D. (1987). Shifter circuits: a computational strategy for dynamic aspects of visual processing. *PNAS*, 84(17):6297 – 6301.
- Arathorn, D. W., Stevenson, S. B., Yang, Q., Tiruveedhula, P., and Roorda, A. (2013). How the unstable eye sees a stable and moving world. *Journal of Vision*, 13(10):22–22.
- Bengio, Y., Courville, A., and Vincent, P. (2014). Representation learning: A review and new perspectives.
- Biederman, I. and Cooper, E. (1991). Evidence for complete translational and reflectional invariance in visual object priming. *Perception*, 20:585 – 593.
- Burwick, T. (2014). The binding problem. *WIREs Cognitive Science*, 5(3):305–315.
- Cossell, L., Iacaruso, M. F., Muir, D. R., Houlton, R., Sader, E. N., Ko, H., Hofer, S. B., and Mrsic-Flogel, T. D. (2015). Functional organization of excitatory synaptic strength in primary visual cortex. *Nature*, 518(7539):399–403.
- Dohare, S., Hernandez-Garcia, J. F., Lan, Q., Rahman, P., Mahmood, A. R., and Sutton, R. S. (2024). Loss of plasticity in deep continual learning. *Nature*, 632(8026):768–774. Editorial: <https://www.nature.com/articles/d41586-024-02525-z>.
- Fukushima, K. (1980). Neocognitron: A self-organizing neural network model for a mechanism of pattern recognition unaffected by shift in position. *Biological Cybernetics*, 36(4):193–202.
- Geman, S. and Geman, D. (1984). Stochastic relaxation, Gibbs distributions and the Bayesian restoration of images. *IEEE Trans. on Patt. Anal. & Mach. Intel.*, PAMI-6:721–741.
- Greff, K., van Steenkiste, S., and Schmidhuber, J. (2020). On the binding problem in artificial neural networks.
- Grill-Spector, K. and Malach, R. (2004). The human visual cortex. *Annual Review of Neuroscience*, 27(1):649–677.
- Hebb, D. O. (1949). *The Organization of Behavior; A Neuropsychological Theory*.
- Hinton, G. and Salakhutdinov, R. (2006). Reducing the dimensionality of data with neural networks. *Science (New York, N.Y.)*, 313:504–7.
- Hinton, G. E. (1981). A Parallel Computation that Assigns Canonical Object-Based Frames of Reference. In *International Joint Conference on Artificial Intelligence*, pages 683–685.
- Hinton, G. E. and Sejnowski, T. J. (1983). Optimal perceptual inference. In *Proceedings of the IEEE Conference on Computer Vision and Pattern Recognition*.
- Hochreiter, S. and Schmidhuber, J. (1997). Long Short-Term Memory. *Neural Computation*, 9(8):1735–1780.
- Hopfield, J. J. (1982). Neural networks and physical systems with emergent collective computational abilities. *Proceedings of the National Academy of Sciences*, 79(8):2554–2558.
- Ito, M., Tamura, H., Fujita, I., et al. (1995). Size and position invariance of neuronal responses in monkey inferotemporal cortex. *Journal of Neurophysiology*, 73(1):218 –226.
- Kingma, D. and Ba, J. (2015). Adam: A method for stochastic optimization. In *International Conference on Learning Representations (ICLR)*, San Diego, CA, USA.
- Kree, R. and Zippelius, A. (1988). Recognition of topological features of graphs and images in neural networks. *J. Phys. A*, 21:813–818.
- LeCun, Y., Bengio, Y., and Hinton, G. (2015). Deep learning. *Nature*, 521(7553):436–444.
- LeCun, Y., Boser, B., Denker, J. S., et al. (1989). Backpropagation Applied to Handwritten Zip Code Recognition. *Neural Computation*, 1(4):541–551.
- Leuba, G. and Kraftsik, R. (1994). Changes in volume, surface estimate, three-dimensional shape and total number of neurons of the human primary visual cortex from midgestation until old age. *Anat Embryol*, 190:351–366.
- Memisevic, R. and Hinton, G. E. (2010). Learning to represent spatial transformations with factored higher-order boltzmann machines. *Neural Computation*, pages 1473–1492.
- Mumford, D. (2003). Pattern theory: the mathematics of perception. In *ICM 2002 · Vol. III · 1–3*, pages 1–21.

- Olshausen, B., CH, A., and Van Essen, D. (1995). A multiscale dynamic routing circuit for forming size- and position-invariant object representations. *Journal of Computational Neuroscience*, 2:45–62.
- Olshausen, B. A. and Field, D. J. (1996). Emergence of simple-cell receptive field properties by learning a sparse code for natural images. *Nature*, 381(6583):607–609.
- Olshausen, B. A. and Field, D. J. (2005). How close are we to understanding v1? *Neural Computation*, 17(8):1665–1699.
- Palm, G. (2013). Neural associative memories and sparse coding. *Neural Networks*, 37:165–171. Twenty-fifth Anniversary Commemorative Issue.
- Prince, S. J. D. (2023). *Understanding Deep Learning*.
- Rosenblatt, F. (1962). *Principles of Neurodynamics: Perceptrons and the Theory of Brain Mechanisms*.
- Simmler, N., Sager, P., Andermatt, P., et al. (2021). A Survey of Un-, Weakly-, and Semi-Supervised Learning Methods for Noisy, Missing and Partial Labels in Industrial Vision Applications. In *Proceedings of the 8th Swiss Conference on Data Science*, pages 26–31.
- Taubman, D. and Marcellin, M. (2002). *Jpeg-2000 image compression: fundamentals, standards and practice*. Kluwer Academic Publishers, Dordrecht.
- Treisman, A. and Schmidt, H. (1982). Illusory conjunctions in the perception of objects. *Cognitive Psychology*, 14(1):107–141.
- Tsodyks, M. and Feigel'man, M. (2007). The enhanced storage capacity in neural networks with low activity level. *EPL (Europhysics Letters)*, 6:101.
- Vaswani, A., Shazeer, N., Parmar, N., Uszkoreit, J., Jones, L., Gomez, A. N., Kaiser, L., and Polosukhin, I. (2017). Attention is All you Need. In *Proceedings of the 31st International Conference on Neural Information Processing Systems*, volume 30, page 6000–6010.
- von der Malsburg, C. (1981). The correlation theory of brain function. Internal Report 81-2, Max-Planck-Institut für Biophysikalische Chemie.
- von der Malsburg, C. (2024). How are segmentation and binding computed and represented in the brain? *Cognitive Processing*, 25(1):67–72.
- von der Malsburg, C., Stadelmann, T., and Grewe, B. F. (2022). A Theory of Natural Intelligence. *arXiv*, (preprint arXiv:2205.00002).
- Waibel, A., Hanazawa, T., Hinton, G. E., et al. (1987). Phoneme Recognition Using Time-Delay Neural Networks. In *Meeting of the Institute of Electrical*, volume 37, pages 329–339.
- Wiskott, L., Fellous, J.-M., Kuiger, N., et al. (1997). Face recognition by elastic bunch graph matching. *IEEE Transactions on Pattern Analysis and Machine Intelligence*, 19(7):775–779.
- Wolfrum, P., Wolff, C., Lücke, J., et al. (2008). A recurrent dynamic model for correspondence-based face recognition. *Journal of Vision*, 8(7):34.